



Supporting Online Material for
Strong Interactions in Multimode Random Lasers

Hakan E. Türeci,* Li Ge, Stefan Rotter, A. Douglas Stone

*To whom correspondence should be addressed. E-mail: tureci@phys.ethz.ch

Published 2 May 2008, *Science* **320**, 643 (2008)
DOI: 10.1126/science.1155311

This PDF file includes:

Materials and Methods
Figs. S1 to S3
References

Strong Interactions in Multimode Random Lasers: Supporting Online Material

Hakan E. Türeci^{1*}, Li Ge², Stefan Rotter^{2†}, A. Douglas Stone²

¹Institute of Quantum Electronics, ETH Zürich, 8093 Zürich, Switzerland

²Department of Applied Physics, P. O. Box 208284,
Yale University, New Haven, CT 06520-8284, USA

*To whom correspondence should be addressed; E-mail: tureci@phys.ethz.ch.

†Presently on leave from Technische Universität Wien,
Wiedner Hauptstraße 8-10/136, A-1040 Vienna, Austria, EU

Materials and Methods 1: Derivation and solution of the self-consistent equations – Details of the algorithm

Derivation of the self-consistent multimode laser equations. The Green function which forms the kernel of the fundamental self-consistent equation Eq. 1 has a non-hermitian spectral representation of the form (S1)

$$G(\mathbf{x}, \mathbf{x}'; k) = \sum_{m=1}^{\infty} \frac{\varphi_m(\mathbf{x}, k) \bar{\varphi}_m^*(\mathbf{x}', k)}{2 k_a(k - k_m(k))}. \quad (\text{S1})$$

where the CF states $\varphi_m(\mathbf{x}, k)$ satisfy the equation

$$-\frac{1}{\epsilon(\mathbf{x})} \nabla^2 \varphi_m(\mathbf{x}, k) = k_m^2(k) \varphi_m(\mathbf{x}, k) \quad (\text{S2})$$

with the boundary condition that outside the gain region there are only outgoing waves with wavevector k . The biorthogonal partners $\bar{\varphi}_m(\mathbf{x}, k)$ satisfy the complex conjugate equation with incoming wave boundary conditions, hence $\bar{\varphi}_m(\mathbf{x}, k) = (\epsilon(\mathbf{x})\varphi_m(\mathbf{x}, k))^*$. The biorthogonality condition on these functions is $\int_{\text{gain}} d\mathbf{x} \bar{\varphi}_m^*(\mathbf{x}, k) \varphi_n(\mathbf{x}, k) = \delta_{mn}$ with appropriate normalization. Writing $G(\mathbf{x}, \mathbf{x}'; k)$ in Eq. 1 in the form Eq. S1, substituting the CF expansion of the unknown lasing modes $\Psi_\mu(\mathbf{x}) = \sum_{m=1}^{\infty} a_m^\mu \varphi_m(\mathbf{x}, k_\mu)$, using the biorthogonality relation and

truncating to N_{CF} CF states nearest the atomic line (gain center) yields Eq. 2, with the non-linear operator $T_{mn}^\mu = T_{mn}(k_\mu; \mathbf{a}^\mu)$ where

$$T_{mn}(k; \mathbf{a}^\mu) = \frac{i\gamma_\perp}{\gamma_\perp - i(k - k_a)} \frac{1}{2k_a(k - k_m(k))} \times \int d\mathbf{x}' \frac{(1 + d_0(\mathbf{x}')) \bar{\varphi}_m^*(\mathbf{x}', k) \varphi_n(\mathbf{x}', k)}{\epsilon(\mathbf{x}') (1 + \sum_\nu \Gamma_\nu |\Psi_\nu(\mathbf{x}')|^2)}. \quad (\text{S3})$$

We refer to $T_{mn}(k; \mathbf{a}^\mu)$ also as $T_{mn}(k)$ or $T_{mn}(k; D_0)$ in the text in order to emphasize the dependence that is relevant in the discussion.

Threshold Matrices: The set of non-linear equations (2) have the following properties. Below some finite value of the pump D_0 only the trivial solution exists: $\Psi_\mu = 0, \forall \mu$. As D_0 is increased, a series of thresholds are reached at which the number of non-trivial solutions increases by one. If we denote the threshold $D_{th}^{(l)}$ for l -mode lasing there exist l solutions $\{\mathbf{a}^\mu, k_\mu\}$ ($\mu = 1, \dots, l$) for a pump parameter D_0 such that $D_{th}^{(l)} < D_0 < D_{th}^{(l+1)}$. In each of these intervals we assume that l solutions to Eq. 2 exist and find them by a method to be described below.

In order to find the first threshold we consider the linear operator $T_{mn}(k; \mathbf{a}^\mu = 0) \equiv \mathcal{T}^{(0)}(k)$ where

$$\mathcal{T}_{mn}^{(0)}(k) = \frac{i\gamma_\perp}{\gamma_\perp - i(k - k_a)} \frac{1}{2k_a(k - k_m(k))} \int d\mathbf{x}' \frac{(1 + d_0(\mathbf{x}')) \bar{\varphi}_m^*(\mathbf{x}', k) \varphi_n(\mathbf{x}', k)}{\epsilon(\mathbf{x}')} \quad (\text{S4})$$

which is obtained by neglecting the $\sum_\nu \Gamma_\nu |\Psi_\nu(\mathbf{x}')|^2$ term in the denominator of Eq. S3. The resulting linear equation associated with (2) has the form

$$\mathcal{T}^{(0)}(k) \mathbf{a}^\mu = (1/D_0) \mathbf{a}^\mu, \quad (\text{S5})$$

which has solutions (as noted in the text) when an eigenvalue of this matrix, $\lambda_n^{(0)}(k), n = 1, \dots, N_{CF}$, is real and has the value $1/D_0$ (i.e. $D_0 \lambda_n^{(0)} = 1$). Since $\mathcal{T}^{(0)}(k)$ is independent of D_0 , so are its eigenvalues. $\mathcal{T}^{(0)}(k)$ is non-hermitian and has complex eigenvalues for general values of k . Denoting the largest eigenvalue of this matrix by $\lambda_1^{(0)}$, we solve Eq. S5 by tuning k until $\text{Im} [\lambda_1^{(0)}(k = k_1)] = 0$; this determines the threshold $D_{th}^{(1)} = 1/\lambda_1^{(0)}(k = k_1)$. k_1 is the lasing frequency of the first mode at threshold; the corresponding eigenvector of $\mathcal{T}^{(0)}(k)$ gives the projection of the lasing mode onto the CF states, \mathbf{a}^1 , at threshold. The ‘‘length’’ of \mathbf{a}^1 is not determined from Eq. S5 but rises continuously from zero at threshold and is determined by the non-linear equation (2) infinitesimally above threshold. The other, smaller eigenvalues of $\mathcal{T}^{(0)}(k)$ define the non-interacting thresholds for other modes with their frequencies determined by the same reality condition, but the actual thresholds of all higher modes will differ substantially from their non-interacting values due to the non-linear term in Eq. 2 which now comes

into play. The actual lasing frequencies of higher modes have only a weak dependence on D_0 and differ little from their non-interacting values (see Fig. 2, inset).

Above the threshold $D_{th}^{(1)}$ we solve the non-linear Eq. 2 by an iterative method to be described below. Assuming we have this solution in hand at each value of D_0 we can construct the generalized interacting threshold matrix

$$\mathcal{T}_{mn}^{(1)}(k; D_0) = \frac{i\gamma_{\perp}}{\gamma_{\perp} - i(k - k_a)} \frac{1}{2k_a(k - k_m(k))} \int d\mathbf{x}' \frac{(1 + d_0(\mathbf{x}'))\bar{\varphi}_m^*(\mathbf{x}', k)\varphi_n(\mathbf{x}', k)}{\epsilon(\mathbf{x}')(1 + \Gamma(k_1)|\Psi_1(\mathbf{x}')|^2)}. \quad (\text{S6})$$

Here, the D_0 dependence of $\mathcal{T}_{mn}^{(1)}$ derives from the non-linear dependence of \mathbf{a}^{μ} (assumed to be determined by the procedure described further below) on D_0 . We will alternatively use the notation $\mathcal{T}_{mn}^{(1)}(k; \mathbf{a}^{\mu})$ in what follows. If we vary k at fixed D_0 this linear operator will have a real eigenvalue $\lambda_1^{(1)}(k_1) = 1/D_0$ reflecting the existence of the first lasing mode. To find the threshold for the second lasing mode we vary k until its second largest eigenvalue satisfies $\text{Im} \left[\lambda_2^{(1)}(k = k_2) \right] = 0$. Similarly to the non-interacting case, k_2 is the lasing frequency of the second mode and its expected threshold is $D_{th}^{(2)} = 1/\lambda_2^{(1)}(k = k_2)$. This procedure generalizes in the obvious manner to the third and higher thresholds. Our algorithm for calculating the multimode lasing states continuously monitors the relevant threshold matrix as D_0 is varied to determine at each pump power how many lasing modes are turned on. The eigenvalues of these threshold matrices at a fixed D_0 have a smooth flow in the complex plane and we can always associate a particular eigenvalue at an arbitrary k with a particular lasing mode μ (which may not be yet turned on). Henceforth μ is assumed to be ordered according to the order of turn-on. The eigenvalue flow of the non-interacting threshold matrix is illustrated in Fig. S1; note that the initial values of each of the eigenvalues are different, as shown by the star-shaped markers.

Non-linear Solver: The interacting threshold matrix $\mathcal{T}^{(1)}(k; D_0)$ provides us with the starting values of the lasing frequencies k_{μ} and the threshold solution \mathbf{a}^{μ} (up to a proportionality constant) infinitesimally above threshold for the non-linear lasing equations (2). Equation 2 appears to be convenient for iterative solution, but it must be further constrained in order for this procedure to work. $\mathcal{T}_{mn}(k; \mathbf{a}^{\mu})$ is invariant under global phase rotations $\mathbf{a}^{\mu} \rightarrow e^{i\phi}\mathbf{a}^{\mu}$ and (2) only has a unique solution when this overall phase is fixed (the “gauge” is fixed). This phase can be fixed in a trial solution, but it will be changed by each iteration of the equation and so the correct procedure is to allow the trial lasing frequency to flow under iteration so as to maintain the desired global phase of the trial solution. In this manner the interacting lasing frequencies can be found above threshold (note that these frequencies are different from the non-interacting or threshold values). In practice, we choose the gauge by setting $\text{Im} \left[a_{M_{\mu}}^{\mu} \right] = 0$, where M_{μ} is the largest CF component of the eigenvector \mathbf{a}^{μ} of the non-interacting threshold matrix $\mathcal{T}^{(0)}(k)$.

With this important modification the solutions to Eq. 2 are found by increasing D_0 in small steps above the first threshold and solving for the fixed point(s) of the equation, the vectors \mathbf{a}^{μ} , by iteration. For this we use a multi-dimensional root finder based on the Powell hybrid method.

Convergence depends on the quality of the initial approximation which in turn depends on how fine the pump range is discretized. We find that close to the thresholds the rate of convergence is in general slower as would be expected for non-linear systems close to a bifurcation. At each value of D_0 the associated interacting threshold matrix is constructed from the non-zero \mathbf{a}^μ which have been found and monitored to check if the next lasing mode has reached threshold and should be included in the non-linear system. Note that the number of lasing modes is not a monotonically increasing function of D_0 ; we find that lasing modes can “turn-off” due to strong modal interactions, as described below (black mode in Fig. 2 and Fig. S2).

The eigenvalues of the interacting threshold matrices as a function of D_0 are very interesting because they show the strong effects of mode competition. If we plot $D_0\lambda_\mu^{(0)}$ vs. D_0 these are just straight lines intersecting unity at the non-interacting thresholds; the interacting eigenvalues will be sub-linear, leading to much higher thresholds, and some will even be decreasing with increasing D_0 , indicating modes which are completely suppressed by mode competition and might never turn on. This behavior is shown in Fig. S2 below along with the behavior of the lasing frequencies vs. D_0 . Strong mode-mode interactions mediated by gain-saturation can be studied in detail in Fig. S2. For instance we observe that the turn-on of the black mode is delayed from $D_0/D_{0c} \approx 72$ to $D_0/D_{0c} \approx 78$ due to interactions mainly with the orange mode, which turns on earlier. From Fig. S2(B) we see that the frequencies of these two modes shift closer to each other, which increases the interaction and results finally in the turn-off of the black mode at about $D_0/D_{0c} \approx 117$, as seen in Fig. 2 and Fig. S2(A). At this point we observe a kink in the intensity of the orange mode. A similar interaction takes place between the green and purple modes as described in the main text.

Materials and Methods 2: Collective contribution to the laser frequency

Here we provide details leading to Eq. 3 of the main text; in this section, we will measure all frequencies from the atomic transition frequency k_a to simplify the equations (e.g. $k_\mu - k_a \rightarrow k_\mu$). The gauge-fixing condition $\text{Im} [a_{M_\mu}^\mu] = 0$ leads to the following equation for the corresponding lasing frequency (we will set $M_\mu = 1$)

$$k_\mu = \frac{\gamma_\perp(q_1^\mu \text{Re}[A_1^\mu] - \kappa_1^\mu \text{Im}[A_1^\mu])}{(\gamma_\perp + \kappa_1^\mu) \text{Re}[A_1^\mu] - (k_\mu - q_1^\mu) \text{Im}[A_1^\mu]} = \frac{\gamma_\perp(q_1^\mu - \kappa_1^\mu \sigma_\mu)}{(\gamma_\perp + \kappa_1^\mu) - (k_\mu - q_1^\mu) \sigma_\mu}. \quad (\text{S7})$$

Here $k_1^\mu = q_1^\mu - i\kappa_1^\mu$ ($\kappa_1^\mu > 0$) is the CF frequency of the largest contributing CF component,

$$A_1^\mu \equiv \sum_{n=1}^{N_{CF}} a_n^\mu \int d\mathbf{x}' \frac{(1 + d_0(\mathbf{x}')) \bar{\varphi}_1^{\mu*}(\mathbf{x}', k) \varphi_n^\mu(\mathbf{x}', k)}{\epsilon(\mathbf{x}') (1 + \sum_\nu \Gamma_\nu |\Psi_\nu(\mathbf{x}')|^2)}. \quad (\text{S8})$$

and $\sigma_\mu \equiv \text{Im}[A_1^\mu] / \text{Re}[A_1^\mu]$. Equation S7 is exact, but it is useful to make minor approximations in order to get a more easily interpreted result. In our parameter range σ_μ is typically much less

than one and so we can replace k_μ in the denominator of Eq. S7 with its first order approximation (i.e. the result for $\sigma_\mu = 0$), which is $k_\mu^{(0)} = \frac{q_1^\mu}{1 + \kappa_1^\mu / \gamma_\perp}$. This leads to the result of Eq. 3

$$k_\mu \approx k_\mu^{(0)} \left[1 - \tan[\phi_1^\mu] \frac{\kappa_1^\mu}{q_1^\mu} \right], \quad (\text{S9})$$

where $\tan[\phi_1^\mu] = \text{Im}[A_1^\mu] / \text{Re}[A_1^\mu]$ and we identify the collective contribution to the lasing frequencies by $k_\mu^{(c)} = -k_\mu^{(0)} \tan[\phi_1^\mu] \kappa_1^\mu / q_1^\mu$. The first term, $k_\mu^{(0)}$, is well-known from single mode lasing, it represents the pulling of the cavity frequency q_1^μ towards the atomic line ($k_a = 0$ in our current convention). In the fractional finesse limit of a DRL $\kappa_1^\mu > \gamma_\perp$, it alone would give $k_\mu \approx q_1^\mu (\gamma_\perp / \kappa_1^\mu) < q_1^\mu$, i.e. a very large pulling of the lasing frequencies towards the atomic line center. This effect is seen in Fig. 1. However the second term in Eq. S9 is the collective effect due to all the other CF states. This contribution has no analog in conventional lasers and is random in sign, as can be seen in Fig. 1, where some frequencies are pushed towards and others away from the atomic line center due to this term. The size of this effect depends on the magnitude of $\sigma_\mu \equiv \text{Im}[A_1^\mu] / \text{Re}[A_1^\mu]$. As noted, in our parameter range this quantity is small; this is due to a remnant of the biorthogonality relation. Analysis of the quantity A_1^μ related to T_{mn}^μ suggests that at larger values of $k_a R$ and with more lasing modes (higher above threshold) the quantity σ_μ can be large and of arbitrary sign. When this is true the approximation leading to Eq. S9 will not be valid, but from Eq. S7 we see that the lasing frequencies will be dominated by the collective effects of all the CF poles and will not be associated with any single CF state or passive cavity resonance. The results discussed in Materials and Methods 4 below support this conjecture.

Materials and Methods 3: Numerical calculation of CF modes of the DRL and parameters

In our model for the DRL the region of uniform gain is assumed to be a disk of radius R , on which the differential equation S2 is discretized with a polar mesh $(\rho(i), \phi(j))$, $i = 1, \dots, N_\rho$, $j = 1, \dots, N_\phi$ chosen to be finer than the wavelength of the light $\lambda = 2\pi/k$ (k is eventually to be set to the respective lasing frequencies k_μ). The resulting eigenvalue equation is $\mathcal{L}_{ij} \varphi_m(i, j) = k_m^2(k) \varphi_m(i, j)$ where $\mathcal{L}_{ij} = -\frac{1}{\epsilon(\rho_i, \phi_j)} \nabla_{\rho(i), \phi(j)}^2$, with $\nabla_{\rho(i), \phi(j)}^2$ the discretized Laplacian in polar coordinates, see Ref. (S2). The static dielectric disorder enters the discretized operator at each grid point explicitly via $\epsilon(\rho_i, \phi_j)$ and can thus be chosen at will; in what follows the dielectric function at each grid point takes the values $\epsilon = \epsilon_1 = (1.2)^2$ or $\epsilon = \epsilon_0 = 1$ randomly with roughly 20% coverage of “nanoparticles”. The outgoing CF boundary condition is imposed by continuously connecting the solution of Eq. S2 and its derivative to a superposition of outgoing Hankel functions, $H_m^{(+)}(kR) e^{\pm im\phi}$, on the boundary of the gain-disk. The resulting boundary conditions are k -dependent and can be written as

$$\varphi(N_\rho + 1, \phi_j) = \sum_m a_m [\varphi(N_\rho)] \left(1 + k\delta \frac{H_m^{(+)\prime}(kR)}{H_m^{(+)}(kR)} \right) e^{im\phi_j}. \quad (\text{S10})$$

where $\delta = \rho_{i+1} - \rho_i$ and $a_m[\varphi(N_\rho)]$ are the discrete angular Fourier coefficients of the solution on the last ring $\varphi(N_\rho, \phi_i)$

$$a_m[\varphi(N_\rho)] = \frac{1}{2\pi} \sum_i^{N_\phi} \varphi(N_\rho, \phi_i) e^{-im\phi_i} \quad (\text{S11})$$

This leads to a finite non-hermitian eigenvalue problem depending parametrically on k which is solved by customized linear algebra packages for sparse matrices. Eqs. S10 and S11 are incorporated by adding a $N_\phi \times N_\phi$ block to the discretized Laplacian \mathcal{L}_{ij} which renders it k -dependent. The resulting solutions $\{k_m(k), \varphi_m(\mathbf{x}, k)\}$ are used during the iteration procedure in the construction of the non-linear operators $T_{mn}(k; \mathbf{a}^\mu)$.

The rest of the parameters used in the calculations presented are as following: $\gamma_\perp R = 1$, $k_a R = 30$, $N_{CF} = 16$.

Materials and Methods 4: Spatial structure of lasing modes

The amplitudes \mathbf{a}^μ determine the spatial structure of the lasing modes via

$$\Psi_\mu(\mathbf{x}) = \sum_{m=1}^{N_{CF}} a_m^\mu \varphi_m^\mu(\mathbf{x}).$$

Since these amplitudes evolve continuously from the relevant eigenvectors of the threshold matrices (see discussion above), it is useful to consider their distribution from analysis of these matrices. Construction of the non-interacting threshold matrix $\mathcal{T}^{(0)}$ (for uniform pumping) finds this matrix to be close to diagonal and its eigenvectors to be localized on single CF states, implying that at the first threshold the lasing state is primarily made up of one CF state. The integral in Eq. S4 is not diagonal by biorthogonality due to the factor $\epsilon(\mathbf{x}')$ in the denominator. However, it can be divided into an integral over the region with background dielectric function ϵ_0 and scattering centers with $\epsilon = \epsilon_1$. Adding and subtracting appropriate quantities and using biorthogonality one finds that $\mathcal{T}_{mn}^0 \propto \int d\mathbf{x}' \frac{\bar{\varphi}_m^*(\mathbf{x}', k) \varphi_n(\mathbf{x}', k)}{\epsilon(\mathbf{x}')} = \frac{1}{\epsilon_0} \left[\delta_{mn} - \frac{\epsilon_1 - \epsilon_0}{\epsilon_1} \int_{g_1} d\mathbf{x}' \bar{\varphi}_m^*(\mathbf{x}', k) \varphi_n(\mathbf{x}', k) \right]$, where g_1 denotes the area of the gain region with $\epsilon = \epsilon_1$. The second term here is small due primarily to the fluctuating phases of the CF states, but also due to the smallness of the prefactor and the fact that we have taken $g_1 \approx 20\%$ of the entire gain region. When $\mathcal{T}^{(0)}$ is approximately diagonal, the quantity σ_μ discussed above is small. As a result, at low pump powers for the first lasing mode, $k_\mu \approx k_\mu^{(0)}$ with a small collective contribution.

However, if one analyzes the interacting threshold matrix $\mathcal{T}^{(1)}(k; D_0)$ (and higher ones) one immediately sees that the presence of lasing modes modifies the denominator in a crucial manner: there is now a space-dependent term (the ‘‘hole-burning term’’) which cannot be divided up into two constant regions, but instead varies continuously throughout the gain medium. As this term increases, the threshold matrices and the non-linear operator T_{mn}^μ become more and more non-diagonal, and each lasing mode becomes distributed over many CF states. Sufficiently far

above threshold, due to these interactions, the lasing modes should lose all resemblance to any single CF state. The modes that turn on at higher pump powers tend to be more distributed over several CF states even at threshold due to the less diagonal character of their higher threshold matrices. This is illustrated in Fig. S3 which shows the calculated decomposition in CF states at $D_0/D_{0c} = 123.5035$ of the green mode in Fig. 2. For the mode chosen there are four CF states with a weight greater than 10%. The 3rd CF state here has the maximal contribution of 25.6%, while it is 55.8% at $D_0/D_{0c} = D_{th}^1 = 71.9519$. The detailed behavior here merits further study as to its dependence on size and type of disorder and on $k_a R$.

A second important observation about the spatial structure of the lasing modes is that the amplitude of the lasing modes increase quasi-exponentially towards the gain boundary, see Fig. 4. This is not due to high-Q passive cavity modes spatially localized at the boundary (as it is for whispering gallery modes of uniform spheres or cylinders); here there are no high-Q passive cavity modes at all (see Fig. 1). This effect is due to the high gain needed to initiate lasing in such leaky systems. Full understanding of what determines the growth rate in this two-dimensional case will also require further study.

Materials and Methods 5: “Frequency repulsion” in DRLs

We can now be more precise about the spatial correlation of modes with nearly degenerate frequencies. By construction, $\mathcal{T}_{mn}(k)$ has a real eigenvalue λ_μ equal to $1/D_0$ at the frequencies k_μ for each mode that is lasing. If there were two modes with $k_\mu = k_\nu$, then the complex random matrix $\mathcal{T}_{mn}(k)$ would have an exact accidental degeneracy. Such matrices are a set of measure zero in the ensemble, and instead, as the eigenvalues λ_μ, λ_ν approach each other in the complex plane, there is an avoided crossing and strong mixing of the eigenvectors $\mathbf{a}^\mu, \mathbf{a}^\nu$ (we see this mixing numerically). Strong overlap of $\mathbf{a}^\mu, \mathbf{a}^\nu$ in turn implies strong spatial correlation, strong hole-burning interaction and suppression of the weaker intensity mode by the higher intensity mode. The net effect is an apparent repulsion between lasing frequencies, even though they are not themselves the eigenvalues of a random matrix. The crossing of lasing and non-lasing frequencies (see Fig. 2) does not require degeneracy of the threshold matrix and is allowed.

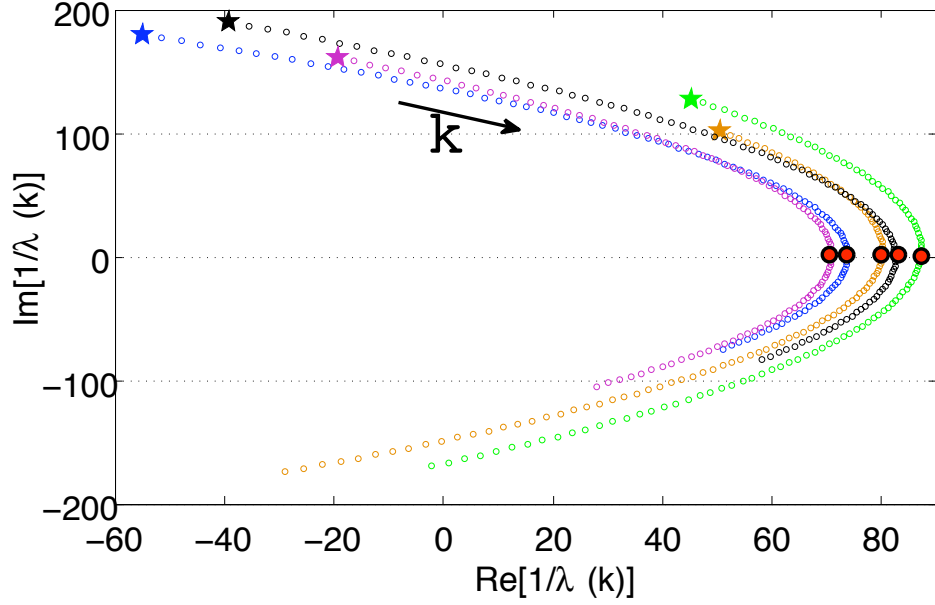


Figure S1: Eigenvalue flow for the non-interacting threshold matrix. Colored circles represent the trajectories in the complex plane of $1/\lambda_\mu(k)$ as a function of k for a scan $k = (k_a - \gamma_\perp, k_a + \gamma_\perp)$ ($k_a R = 30, \gamma_\perp R = 1$). Shown are only a few eigenvalues out of $N_{CF} = 16$ modes included. The direction of flow as k is increased is indicated by the arrow. Star-shapes mark the initial values of $1/\lambda_\mu(k)$ at $k = k_a - \gamma_\perp$. The full red circles mark the values at which the trajectories intersect the real axis, each at a different value of $k = k_\mu$, providing the non-interacting thresholds $D_{th}^{(\mu)}$.

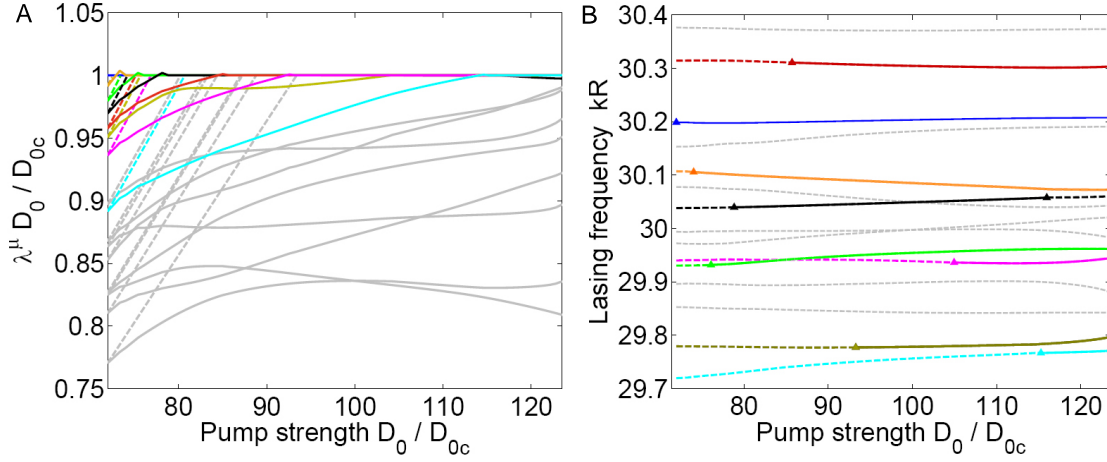


Figure S2: Evolution of the thresholds and lasing frequencies as a function of D_0 . (A) Evolution of the quantities $\lambda_\mu^{(i)} D_0(i)$ as the pump is increased. $\lambda_\mu^{(i)}$ denotes the real λ_μ calculated at step i of the discretization of the full D_0 -range. At a given step i , all modes μ which are below the threshold (delineated by the line $\lambda_\mu D_0 = 1$) are non-lasing at pump $D_0(i)$. Once a mode starts to lase its corresponding value $\lambda_\mu D_0$ is clamped at $\lambda_\mu D_0 = 1$. The full colored lines represent the modes which start lasing within the calculated range of D_0 . The dashed lines represent the evolution $\lambda_\mu^{(0)} D_0(i)$ i.e. the evolution, had mode-mode interactions not existed, while gray lines indicate modes which do not turn on in the pump range shown. The color-coding is identical to that of Fig. 2. (B) Analogous evolution of lasing frequencies k_μ at which $\lambda_\mu^{(i)}(k)$ become real. The non-lasing modes are drawn in dashed lines, turning into full lines as the modes begin to lase. Gray lines represent modes which never lase in the calculated range of D_0 . Note the absence of frequency repulsion of non-lasing modes.

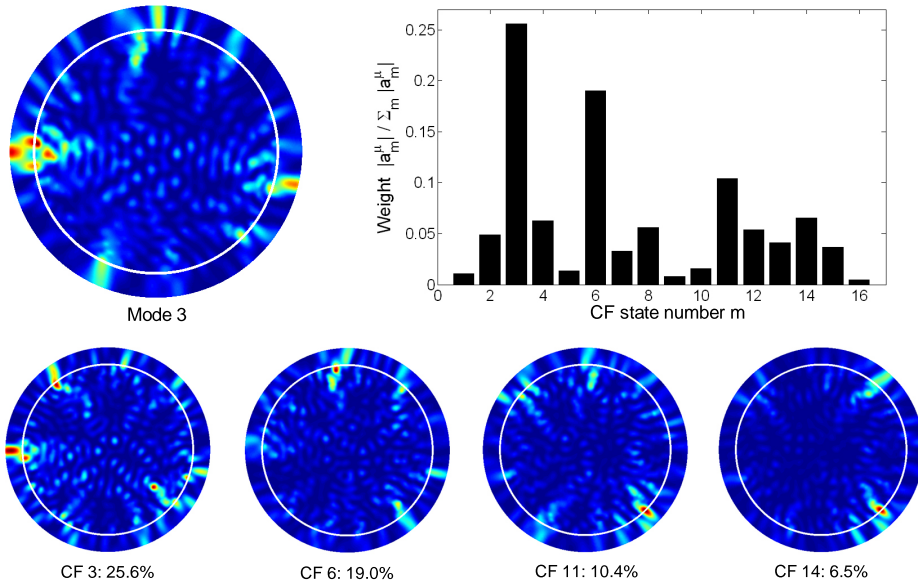


Figure S3: Spatial structure of lasing modes. False color plot of the spatial structure of the third mode (green curve in Fig. 2) and its expansion in the CF basis (upper right) at $D_0/D_{0c} = 123.5035$. The structures of four of the CF states with largest weights are shown at the bottom. The maximum amplitudes of the field distributions in these plots are rescaled to unity to facilitate comparison.

References and Notes

- S1. Analytic formulas in Supporting Online Material have been simplified by assuming k_a is much greater than all other frequencies measured from the atomic line center. This approximation is not necessary and has not been used in the calculations presented.
- S2. S. Rotter, J.-Z. Tang, L. Wirtz, J. Trost, and J. Burgdörfer, Phys. Rev. B **62**, 1950 (2000).